# Dual-Polarized Shaped-Beam Transmitarray to obtain a multi-zone coverage for 5G indoor communications

Álvaro F. Vaquero, *Student Member, IEEE*, Marcos R. Pino, and Manuel Arrebola, *Senior Member, IEEE*

***Abstract*—A dual-polarized transmitarray antenna is proposed to generate a multi-zone coverage at 28 GHz for 5G indoor communications. The transmitarray radiates a constant power density within its near-field region over a specific area generating different spots in dual-polarization. The different spots are produced by feeding the transmitarray with a cluster of horn antennas, which are spatially distributed to obtain beams in different directions. The performance of the coverage is improved with a Phase-Only Synthesis (POS) of the transmission coefficients. The transmitarray is designed with dielectric-only elements, which provides a low-cost solution. The prototype is measured in a planar acquisition range, showing a high agreement with simulations. The proposed transmitarray together with the spatial feed distribution provides a potential alternative to generate multi-zone coverages in millimeter frequencies.**

***Index Terms*—Dielectric transmitarray, phase-only synthesis, near-field coverage, 5G.**

## I. Introduction

FOR 5G communications and especially wireless communications, high energy efficiency is expected to be a key factor in scenarios with multiple users and high data rates. 5G involves increasing the capacity of the system to lead with a massive number of users but also there will be a myriad of other devices such as sensors or electronic appliances, all interconnected. These elements will demand the best performance in terms of bandwidth, data rates, and efficiency. An important challenge in 5G wireless communications is to satisfy the requirements at high frequencies, such as mm-Wave, to provide high-speed wireless cellular networks [1],[2]. At those frequencies, signal propagation has a deep impact on communications, mainly due to the phenomena of path losses and the sensitivity to physical barriers [3]. A reduction in the distance between the 5G elements reduces the paths losses and the number of physical barriers between them. A clear example is found in indoor scenarios whose coverage is provided by a base station, commonly placed far away from users.

The deployment of efficient indoor communication faces both issues since the base station is placed closer to the users, reducing the distance and the physical barriers. The reduction of the distance between the base station and 5G elements produces communications within the near-field region of the base station antenna. Hence, the deployment of efficient indoor communications within the near-field is an indispensable solution to support wireless communications in 5G and beyond. On the other hand, antennas are a key element since the base station must provide the coverage wherein the devices are placed and avoid undesired directions to improve communication efficiency. Therefore, shaped beams are a potential candidate to reach uniform power densities over desired areas that are adapted to the coverage requirements. A suitable candidate is a spatially-fed array (SFA) antennas, in particular reflectarrays and transmitarrays, or even metasurfaces [4],[5]. These antennas are low-profile solutions to reach very compact structures that are easily integrated with indoor scenarios. In addition, different published works have demonstrated the potential of SFA antennas achieving far- and near-field shaped patterns to improve the performance in communications [6]-[8].

In this work, a transmitarray is proposed as a low-cost compact solution to generate a multi-zone coverage at 28 GHz. The transmitarray is designed in a central-single feed configuration to radiate a spot at broadside. The spot is widened using a phase-only near-field synthesis to cover a larger area. Then, the transmitarray is fed by 4 additional feeds to create a multi-zone coverage, so that each feed produces a single spot. The five feeds work as a cluster at the same frequency but orthogonal linear polarizations. This scheme avoids interference between adjacent spots and improves the capacity and the size of the coverage. This work aims to evaluate the shaped beam performance in multi-feed configurations based on the spatial distribution of the feeds. Finally, the transmitarray is manufactured with additive manufacturing and it is evaluated in a planar acquisition range to analyze the coverage performance.

This work was supported in part by the Ministerio de Ciencia, Innovación y Universidades under Project TEC2017-86619-R (ARTEINE); and Ministerio de Ciencia e Innovación and Agencia Española de Investigación within Project ENHANCE-5G (PID2020-114172RB-C21-2/AEI/10.13039/501100011033).

Á. F. Vaquero is with the Department of Signals, Systems and Radiocommunications, Group of Applied Electromagnetics, Universidad Politécnica de Madrid, Madrid, 28040, Spain.

M. R. Pino and M. Arrebola are with the Department of Electrical Engineering, Group of Signal Theory and Communications, Universidad de Oviedo, Gijón, 33203, Spain, (e-mail: arrebola@uniovi.es).

## II. TRANSMITARRAY FOR DUAL-POLARIZED FEMTOCELLS

The transmitted field of a transmitarray on its surface can be expressed as

$$\vec{E}_{trans}(x_m, y_n) = \mathbf{T}^{mn} \cdot \vec{E}_{inc}(x_m, y_n) \quad (1)$$

where $\vec{E}_{inc}$ is the incident field on the opposite surface, $(x_m, y_n)$ are the coordinates of the $(m,n)$th element, and $\mathbf{T}$ the transmission matrix, which fully characterizes the response of the element as

$$\mathbf{T}^{\mathrm{mn}} = \begin{pmatrix} \tau_{xx}^{mn} & \tau_{xy}^{mn} \\ \tau_{yx}^{mn} & \tau_{yy}^{mn} \end{pmatrix} \quad (2)$$

If the elements are modeled as ideal, lossless, and matched phase shifters ($|\tau_{xx}| = |\tau_{yy}| = 1$ and $\tau_{xy} = \tau_{yx} = 0$), $\mathbf{T}^{\mathrm{mn}}$ is simplified to

$$\mathbf{T}^{\mathrm{mn}} = \begin{pmatrix} e^{\phi_{xx}} & 0 \\ 0 & e^{\phi_{yy}} \end{pmatrix} \quad (3)$$

where $\phi_{xx}$ and $\phi_{yy}$ are the phase shifts introduced by an element in X-polarization and Y-polarization, respectively.

According to (1) and (3), the amplitude of the transmitted field only depends on the amplitude of the incident field, and the phase on a combination of the phase response of the cell ($\phi_{xx}$ or $\phi_{yy}$) and the phase of the incident field ($\phi_{inc}$) [9]. The feed is fixed in a single position, thus the incident field is fixed and known beforehand. If the feed changes its position, the incident field changes as well as the transmitted field. If the feed is displaced in a circular arc as Fig. 1 depicts, and the feed is pointing to the geometrical center of the transmitarray, the amplitude of the incident field barely changes in each position [10]. However, the phase of the incident field changes, introducing a different progressive phase onto the transmitarray surface in each position. Mainly, this progressive phase does not modify the shape of the radiated beam but the angular pointing position of the beam. Noting that the cells must be designed to ensure good angular stability to keep the phase response $\phi_{xx}$ and $\phi_{yy}$ through the different impinging waves.

This approach is used to obtain a multi-feed shaped-beam transmitarray antenna. The spatial feed distribution follows the circular-arc path of Fig. 1 to reduce the difference between the amplitude of the different incident fields. This distribution keeps the same distance between the center of the antenna and the phase center of each feed. The spatial feed distribution is defined in the main planes of the transmitarray antenna, taking the focal distance ($f$) of the central feed as the radius of the arc. The circular-arc path can be expressed as

$$(x, y, z) = (f \sin\gamma, 0, -f \cos\gamma) \text{ for the } xoz \text{ plane} \quad (4.1)$$
$$(x, y, z) = (0, f \sin\beta, -f \cos\beta) \text{ for the } yoz \text{ plane} \quad (4.2)$$

where $\gamma$ and $\beta$ are the angular distribution of two adjacent feeds at the $xoz$ and $yoz$ plane, respectively.

## III. ANTENNA DESIGN AND COVERAGE IMPROVEMENT

### A. Antenna optics and coverage definition

The transmitarray is made up of 576 elements in a regular distribution of 24×24 cells with a periodicity of 5×5 mm$^2$. The side of the antenna is 120 mm; therefore, the equivalent aperture

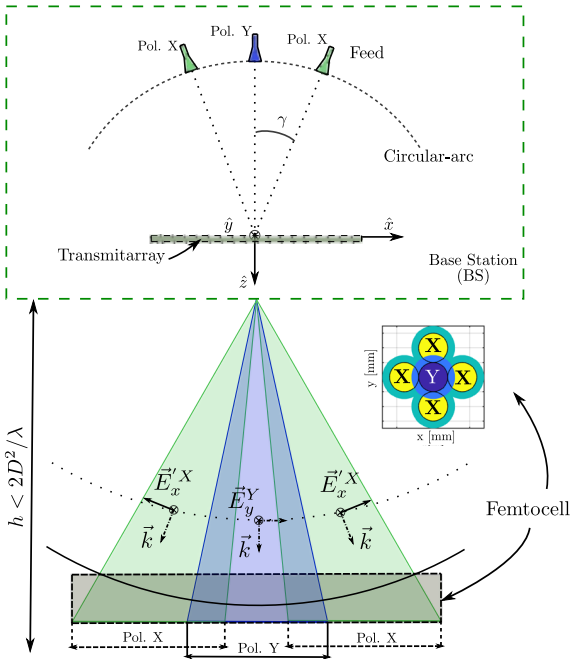


Fig. 1. Cross sectional view of the spatial distribution of the feeds defined in the circular-arc path.

is 169.7 mm$^2$. The central feed is located at 100 mm providing a relatively compact structure with an $f/D = 0.58$. The feed is a standard gain horn of 15 dBi gain working on the linear polarization Y according to Fig. 1 at 28 GHz. The other four feeds are distributed according to (4). The feeds are separated on angular distribution of $\pm 15°$ around the central feed. These four feeds are standard gain horns of 15 dBi but working in the X linear polarization at 28 GHz, which is orthogonal to the polarization of the central feed.

Conversely, the multi-zone coverage is defined on a $xoy$ plane at a distance of $z$ = 1.80 from the center of the transmitarray, thus the coverage is within the near-field of the antenna according to $2D^2/\lambda$. Each feed radiates a different spot obtaining the polarization scheme shown in Fig. 1. The goal is to provide a multi-zone coverage wherein the radiated power density is constant, increasing the area that may be reached with a single feed. The maximum amplitude ripple to consider the coverage area constant is 3 dB. The spots can be generated in both linear polarizations. However, the external spots are overlapped with the central spot and a scheme to minimize the interferences is chosen. In this case, orthogonal polarizations are proposed (see Fig. 1).

### B. Evaluation and improvement of the femtocell

As a first approach, a far-field focused transmitarray is evaluated to generate the different spots of Fig. 1. The transmitarray is designed considering the central feed and radiating a beam in boresight direction ($\theta_0 = 0°, \varphi_0 = 0°$) for Y polarization according to

$$\phi_{yy}(x_m, y_n) = \phi_{inc}(x_m, y_n) - k_0(x_m cos\varphi_0 + y_n sin\varphi_0) sin\theta_0 \quad (5)$$

where $\phi_{yy}(x_m, y_n)$ is the phase of the transmission

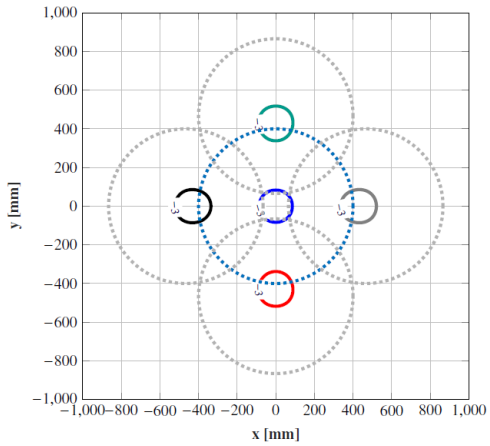


Fig. 2. Evaluation of the radiated femtocell by a far-field focused transmitarray using five horns. The central spot operates on Y polarization whilst the others on X polarization. Dotted lines are the required −3 dB contour.

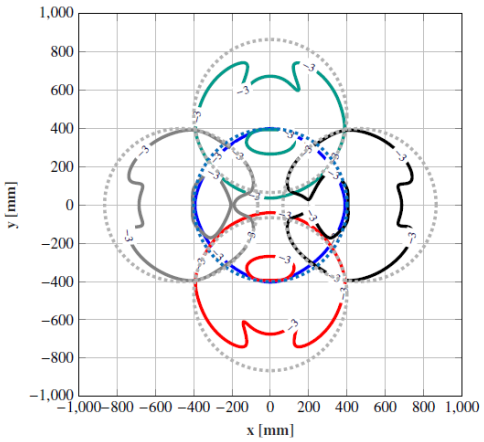


Fig. 3. Evaluation of the radiated femtocell after the optimization process using the five horns. The central spot works on Y linear polarization whilst the others on X polarization. Dotted lines are the required −3 dB contour.

coefficient of the $(m,n)th$-element, $\phi_{inc}^{mn}$ is the phase of the incident field on the element; $k_0$ is the vacuum wavenumber; and $\theta_0$ and $\varphi_0$ are the pointing direction.

According to Fig. 1, the central spot is defined in $Y$ polarization, and (5) provides the phase of the transmission coefficients for this polarization. However, if the transmitarray element behaves similarly in both polarizations, the transmitarray response would not be affected by the feed polarization. The multi-zone coverage is evaluated using the whole cluster and the resulting near-field is shown in Fig. 2. As expected, the five spots are perfectly collimated in the desired directions, demonstrating that the angular distribution of the cluster leads to the same angular distribution of the spots regardless of the polarization. However, none of these spots are overlapped to its adjacent and a constant radiated power density is not achieved.

To improve the multi-zone coverage and achieve a continuous field distribution, the phase of the transmission coefficients $\phi_{yy}(x_m, y_n)$ are synthesized using a Phase-Only Synthesis (POS). The POS is based on the generalized Intersection Approach (gIA) [11]. The gIA is modified to compute the near-field radiated within the near-field [12] instead of the far-field. Hence, this approach allows directly imposing the constraints in the amplitude of the radiated near-field [13]. The specifications are imposed at the coverage plane at $z = 1.8$ m, establishing a maximum ripple of 3 dB within a circular area of radius 400 mm. This process aims to widen the central spot to cover it with a uniform field distribution. The synthesis process is divided into a multi-stage strategy which requires to carry out different synthesis with the gIA. In each new synthesis the specifications are tightened, starting from a laxer ripple within a shorter area to the final ones. Then, the multi-zone coverage will be evaluated to evaluate whether the external spots are also improved because of the spatial feed distribution.

After the synthesis process, a new phase distribution $\phi'_{yy}(x_m, y_n)$ is obtained and the new multi-zone coverage is shown in Fig. 3. The central beam has been notably widened from 5.72° to 26.66°, considering the 3 dB decay. The radiated power density within this spot is mostly flat with a ripple lower than 1.5 dB. The lateral spots are also widened to 12.72° if the overlapped area is not considered. These spots present a certain distortion and are not widened as the central spot since they have not been included in the optimization process. However, this approach reaches a constant coverage area of 52.10°, which is a 914% regarding the initial phase distribution and an 89.80% more than using a single feed.

The POS considers the elements as ideal phase-shifters that only introduce a certain delay. The angle of incidence of the element changes from one feed to the other. Thus, the response of the element is different for each feed. To include constraints in the adjacent spots and minimize the distortion, a full characterization of the element must be included in the gIA, for each feed. This approach (POS plus feed distribution) notably decreases in complexity a multi-target optimization in which all the spots are included.

### C. *Transmitarray design*

Once a solution that satisfies the desired femtocell is reached, the phase of the transmission coefficients $\phi'_{yy}(x_m, y_n)$ must be designed properly to introduce the desired phase-shifts. To operate in dual polarization the elements must introduce the same phase-shift in both polarizations. The proposed elements are based on a dielectric-only solution which provides a low-cost and additive manufacturing solution. These elements are square dielectric prisms of dimensions $(\lambda/2\ (a) \times \lambda/2\ (a) \times 2\lambda\ (t))$ and an embedded airgap [14] (see Fig. 4). The airgap is a square air prism of variable dimensions $(W \times W \times L)$ in order to control the infill of the cell and its dielectric effective constant $(\epsilon_{eff})$. The variation of the $\epsilon_{eff}$controls the phase-shift introduced by the cell. This element provided a phase-shift range of 360°, which is enough to physically implement a whole phase cycle at 28 GHz. Only the elements with transmission losses lower than 1.5 dB are used in the design.

In the design the dimensions of the airgaps are adjusted, element by element, considering local periodic environment and the real angle of incidence [14]. The output of this process

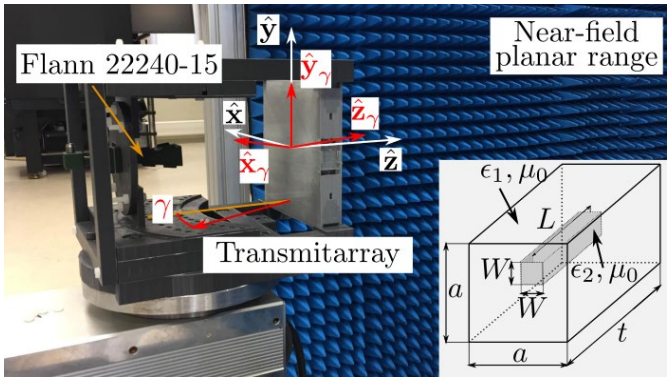


Fig. 4. Setup at the planar acquisition range to evaluate the multi-zone of the proposed prototype. The feed horn can be placed at the different prescribed placements, and a sketch of the selected cell is included.

is a layout of dielectric-only cells that minimize the differences between the phase-shift of the cell and the required one ($\phi'_{yy}(x_m, y_n)$). The behavior of these cells is the same in both linear polarizations.

## IV. Experimental Validation

The transmitarray has been manufactured using a Fused Deposition Modeling (FDM) technique, which is a 3D printing technique based on the melting and layer-by-layer deposition of a thermoplastic polymer, PLA ($\epsilon_r = 2.95, \tan\delta = 0.015$) [15], through a nozzle tip. Then, the prototype has been measured in the planar acquisition range at the Universidad de Oviedo. Due to physical limitations on the facilities, the near-field pattern is not directly evaluated at the coverage plane. The near-field is measured at 100 mm from the antenna aperture within a regular grid of 120×120 mm$^2$, which is large enough to capture most of the electric field. Then, the near-field at the coverage plane (1.80 m) is obtained using a transformation based on Spherical Wave Expansion (SWE) with GRASP [16]. A PLA structure holds the transmitarray antenna and the feed is a horn antenna of 15 dBi gain (Flann 22240-15). The cluster is simulated using this horn antenna and moving it to the different required positions (see Fig. 4). The probe is an open-ended waveguide at Ka-band.

The 3 dB contour of the measured spots at 28 GHz is shown in Fig. 5, obtaining a good agreement between with simulations. The central spot behaves as simulation results with a total width of 20.6° and a ripple lower than 1.5 dB within this area. The lateral spots present a similar shape to simulations. However, despite having the distortion the spots are widened to 11.48º, considering the 3 dB decay without the overlapped area. The total area of the multi-zone coverage is 44.6°, which is more than the 85% of the simulated femtocell.

The slight differences with simulations are associated with the response of the cell. The POS is carried out modeling the elements as ideal phase-shifters and two effects are not considered in advance. First, the losses of the dielectric material and the mismatch in the dielectric-air interface, which mainly affect the size of the central spot. Second, the angular response of the cell adds some distortion to the beam shaping, which is appreciable in the lateral spots.

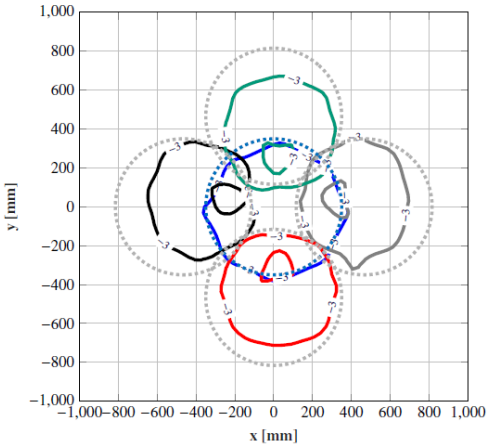


Fig. 5. Evaluation of the measured femtocell at 28 GHz after the optimization process using the five horns. The central spot works on Y linear polarization whilst the others on X polarization. Dotted lines are the required −3 dB contour.

Although the coverage is synthesized in a single plane, the planes close to 1.8 m should behave similar. Therefore, the multi-zone behavior may be found not on a single plane but on a volume. In this case, the coverage has been evaluated from 1.65 to 2.0 m, obtaining a constant near-field power density through a range of 44.6º and a depth of 350 mm.

## V. Conclusion

A transmitarray working at 28 GHz has been presented to generate near-field femtocell for 5G indoor communications. The transmitarray is designed considering a single feed working on a centered configuration and a single linear polarization. Then, four different feeds are added to feed the transmitarray with a cluster of horn antennas. These extra four horn antennas work at the same frequency but orthogonal linear polarization regarding the central feed. In a first approach, a far-field focused transmitarray is evaluated. However, this solution does not provide a continuous near-field which can be considered a femtocell. Hence, the transmitarray is optimized using a POS based on the generalized Intersection Approach for near-field. This process aims to widen the central spot but only the central feed is considered. Although a multifocal optimization could be carried out to design the entire antenna at once, the approach proposed in this work decreases in complexity a multi-target optimization. Moreover, due to the proposed spatial distribution of the cluster the other spots are also improved. After this process, the transmitarray generates a femtocell of 52.10° on dual polarization. Then, the transmitarray is manufactured using a 3D printing technique and dielectric-only elements, which provides a low-cost and easy-manufactured antenna. This prototype is evaluated in a planar acquisition range and the results show a very good agreement with simulations. The measured femtocell shows an angular range of 44.6° through a volume, at least, of 350 mm. This approach provides a compact, low-cost antenna to generate wide-angle dual-polarization near-field femtocells.

## REFERENCES


[1] T. S. Rappaport *et al.*, "Millimeter Wave Mobile Communications for 5G Cellular: It Will Work!," *IEEE ACCESS*, vol. 1, pp. 335-349, 2013.

[2] T. S. Rappaport, G. R. MacCartney, M. K. Samimi, and S. Sum, "Wideband Millimeter-Wave Propagation Measurements and Channel Models for Future Wireless Communication System Design," in *IEEE Transactions on Communications.*, vol. 63, no. 9, pp. 3029-3056, Sept. 2015.

[3] S. Salous, *et al.*, "Millimeter-Wave Propagation : Characterization and modeling towards 5G systems," *IEEE Antennas and Propag. on Magazine*, vol. 58, no. 6, pp. 115-127, Dec. 2016.

[4] P. Zhang, L. Li, X. Zhang, H. Liu, and Y. Shi, "Design, Measurement and Analysis of Near-Field Focusing Reflective Metasurface for Dual-Polarization and Multi-Focus Wireless Power Transfer," in *IEEE Access*, vol. 7, pp. 110387-110399.

[5] O. Quevedo-Teruel, J. Miao, M. Mattsson, A. Algaba-Brazalez, M. Johansson and L. Manholm, "Glide-Symmetric Fully Metallic Luneburg Lens for 5G Communications at Ka-band," in *IEEE Antennas Wirel. Propag. Lett.*, vol. 17, no. 9, pp. 1588-1592, Sept. 2018.

[6] C. Xue, W. Lou and N. Chen, "Broadband Double-Layered Huygens' Metasurface Lens Antenna for 5G Millimeter-Wave Systems," in *IEEE Trans. Antennas and Propag.*, vol. 68, no. 3, pp. 1468-1476, March 2020.

[7] S. A. Matos *et al.*, "3-D-Printed Transmit-Array Antenna for Broadband Backhaul 5G Links at V-Band," in *IEEE Antennas Wirel. Propag. Lett.,* vol. 19, no. 6, pp. 977-981, June 2020.

[8] P. Robustillo, J. Zapata, J. A. Encinar, and M. Arrebola, "Design of a Contoured-Beam Reflectarray for a EuTELSAT European Coverage Using a Stacked-Patch Element Characterized by an Artificial Neural Network," in *IEEE Antennas Wirel. Propag. Lett.*, vol. 11m pp. 977-980, 2012.

[9] C. C. Cruz, C. A. Fernandes, S. A. Matos and J. R. Costa, "Synthesis of Shaped-Beam Radiation Patterns at Millimeters-Waves Using Transmit Arrays," in *IEEE Trans. Antennas Propag.,*vol. 66, no.8, pp. 4017-4024, Aug. 2018.

[10] M. Arrebola, J. A. Encinar, and M. Barba, "Multifed Printed Reflectarray With Three Simultaneous Shpaed Beams for LMDS Central Station Antenna," in *IEEE Trans. Antennas and Propag.*, vol. 56, no. 6, pp. 1518-1527, June 2008.

[11] D. R. Prado, Á. F. Vaquero, M. Arrebola, M. R. Pino, and F. Las-Heras, "Acceleration of Gradient-Based Algorithms for Array Synthesis With Far-Field or Near-Field Constraints", in *IEEE Trans. Antennas Propag.,* vol. 66, no. 10, pp. 5239-5248, Oct 2018.

[12] Á. F. Vaquero, M. Arrebola, M. R. Pino, R. Florencio, and J. A. Encinar, "Demonstration of a Reflectarray with Near-field Amplitude and Phase Constraints as Compact Antenna Test Range Probe for 5G New Radio Devices", in *IEEE Trans. Antennas Propag.,* vol. 69, no. 5, pp. 2715-2726, May 2021.

[13] Á. F. Vaquero, D. R. Prado, M. Arrebola, M. R. Pino and F. Las-Heras, "Near field synthesis of reflectarrays using intersection approach," *2017 11th European Conference on Antennas and Propagation (EUCAP)*, Paris, 2017, pp. 3644-3648.

[14] Á. F. Vaquero, M. R. Pino, M. Arrebola, S. A. Matos, J. R. Costa and C. A. Fernandes, "Bessel Beam Generation Using Dielectric Planar Lenses at Millimeter Frequencies," in *IEEE Access*, vol. 8, pp. 216185-216196, 2020.

[15] J. M. Felicio, C. A. Fernandez, and J. R. Costa, "Complex permittivity and anisotropy measurement of 3D-printed PLA at microwaves and millimeter-waves," in *Proc. 22nd Int. Conf. Appl. Electromagn. Commun. (ICECOM)*, Dubrovnik, Croatia, Sep. 2016, pp. 1-6.

[16] *GRASP V10,* TICRA, Copenhagen, Denmark, 2016.